nature genetics

INPP5E mutations cause primary cilium signaling defects, ciliary instability and ciliopathies in human and mouse

Monique Jacoby[1,11], James J Cox[2,11], Stéphanie Gayral[1,11], Daniel J Hampshire[3], Mohammed Ayub[4], Marianne Blockmans[1], Eileen Pernot[1], Marina V Kisseleva[5], Philippe Compère[6], Serge N Schiffmann[7], Fanni Gergely[8], John H Riley[9], David Pérez-Morga[10], C Geoffrey Woods[2,11] & Stéphane Schurmans[1,11]

The primary cilium is an antenna-like structure that protrudes from the cell surface of quiescent/differentiated cells and participates in extracellular signal processing[1–3]. Here, we report that mice deficient for the lipid 5-phosphatase Inpp5e develop a multiorgan disorder associated with structural defects of the primary cilium. In ciliated mouse embryonic fibroblasts, Inpp5e is concentrated in the axoneme of the primary cilium. Inpp5e inactivation did not impair ciliary assembly but altered the stability of pre-established cilia after serum addition. Blocking phosphoinositide 3-kinase (PI3K) activity or ciliary platelet-derived growth factor receptor α (PDGFRα) restored ciliary stability. In human *INPP5E*, we identified a mutation affecting INPP5E ciliary localization and cilium stability in a family with MORM syndrome, a condition related to Bardet-Biedl syndrome. Together, our results show that INPP5E plays an essential role in the primary cilium by controlling ciliary growth factor and PI3K signaling and stability, and highlight the consequences of INPP5E dysfunction.

Lipid 5-phosphatases selectively remove the phosphate from position D-5 of the inositol ring of phosphoinositides and inositolphosphates[4,5]. To characterize the functions of the 5-phosphatase Inpp5e[6–8], we generated *Inpp5e*$^{\Delta/+}$ mice (**Supplementary Fig. 1a**). We obtained no adult *Inpp5e*$^{\Delta/\Delta}$ mutant mice from intercrosses between *Inpp5e*$^{\Delta/+}$ mice. However, at embryonic day 13.5 (E13.5) and E18.5, 16.9% (11/65) and 14.8% (12/81) of embryos were homozygous for the deletion allele, respectively. The mutant mice died soon after birth, indicating that total inactivation of Inpp5e led to embryonic and postnatal death. Analyses confirmed the absence of Inpp5e protein in mutant cells and tissues (**Fig. 1a**). *Inpp5e*$^{\Delta/\Delta}$ mice presented with bilateral anophthalmos (100%, $n = 43$) and postaxial hexadactyly (62.5%, $n = 16$; **Fig. 1b,c**). Histological analyses revealed that eye development ceased at the optic vesicle stage, just before the appearance of the optic cup (**Fig. 1d**). Analysis of kidneys from the mice revealed the presence of multiple cysts (100%, $n = 10$; **Fig. 1e**). Of the cysts, 84% expressed AQP2 and 14% expressed AQP1, indicating an origin in cortical collecting and connecting ducts (when AQP2$^+$) as well as proximal tubules and the descending limb of the loop of Henle (when AQP1$^+$) (**Supplementary Fig. 2**). Only 2% of the renal glomeruli were cystic. *Inpp5e*$^{\Delta/\Delta}$ embryos had skeletal abnormalities such as a bifid sternum (50%, $n = 6$), delayed ossification of metacarpals and phalanges (100%, $n = 5$) and cleft palate (75%, $n = 4$; **Fig. 1f–h**). We identified cerebral developmental defects, such as anencephaly and exencephaly, in 30% of *Inpp5e*$^{\Delta/\Delta}$ embryos at E15.5 ($n = 30$; **Fig. 1i,j**). We did not detect liver alterations, laterality defects or respiratory cilium defects in mutant animals. The tissue localization of lesions observed in *Inpp5e*$^{\Delta/\Delta}$ embryos matched the tissue expression of *Inpp5e* mRNA during mouse embryogenesis (**Supplementary Fig. 3**).

Because most of the defects in *Inpp5e*$^{\Delta/\Delta}$ mice are features of ciliopathies[1–3,9–11], we investigated primary cilia in renal tubular cells from these mice (**Fig. 2**). Primary cilia protruding from renal cells lining *Inpp5e*$^{+/+}$ tubules and *Inpp5e*$^{\Delta/\Delta}$ noncystic tubules were similar in number and morphology; however, in the renal cysts of *Inpp5e*$^{\Delta/\Delta}$ embryos, the number, size and morphology of primary cilia were markedly altered (**Fig. 2a–c**). Scanning electron microscopy (SEM) revealed that cilia were sparse and appeared dilated. Dilation

[1]Institut de Recherches Interdisciplinaires en Biologie Humaine et Moléculaire (IRIBHM), Institut de Biologie et de Médecine Moléculaires (IBMM), Université Libre de Bruxelles, Gosselies, Belgium. [2]Department of Medical Genetics, Cambridge Institute of Medical Research, Wellcome/MRC Building, Addenbrooke's Hospital, Cambridge, UK. [3]Academic Unit of Haematology, Henry Wellcome Laboratories for Medical Research, School of Medicine and Biomedical Sciences, University of Sheffield, Sheffield, UK. [4]Psychiatry of Learning Disability, St. Lukes Hospital, Middlesbrough, UK. [5]Division of Hematology, Washington University School of Medicine, St. Louis, USA. [6]Cellule d'Appui Technologique en Microscopie, Institut de Chimie, Université de Liège, Liège, Belgium. [7]Laboratoire de Neurophysiologie, Université Libre de Bruxelles, Bruxelles, Belgium. [8]Cancer Research UK, Cambridge Research Institute, Li Ka Shing Centre, University of Cambridge, Cambridge, UK. [9]GSK Respiratory Medicines Development Centre, Stockley Park, Uxbridge, UK. [10]Laboratoire de Parasitologie Moléculaire, Institut de Biologie et de Médecine Moléculaires (IBMM), Université Libre de Bruxelles, Gosselies, Belgium. [11]These authors contributed equally to this work. Correspondence should be addressed to S.S. (sschurma@ulb.ac.be) or C.G.W. (cw347@cam.ac.uk).

Received 25 November 2008; accepted 15 June 2009; published online 9 August 2009; doi:10.1038/ng.427

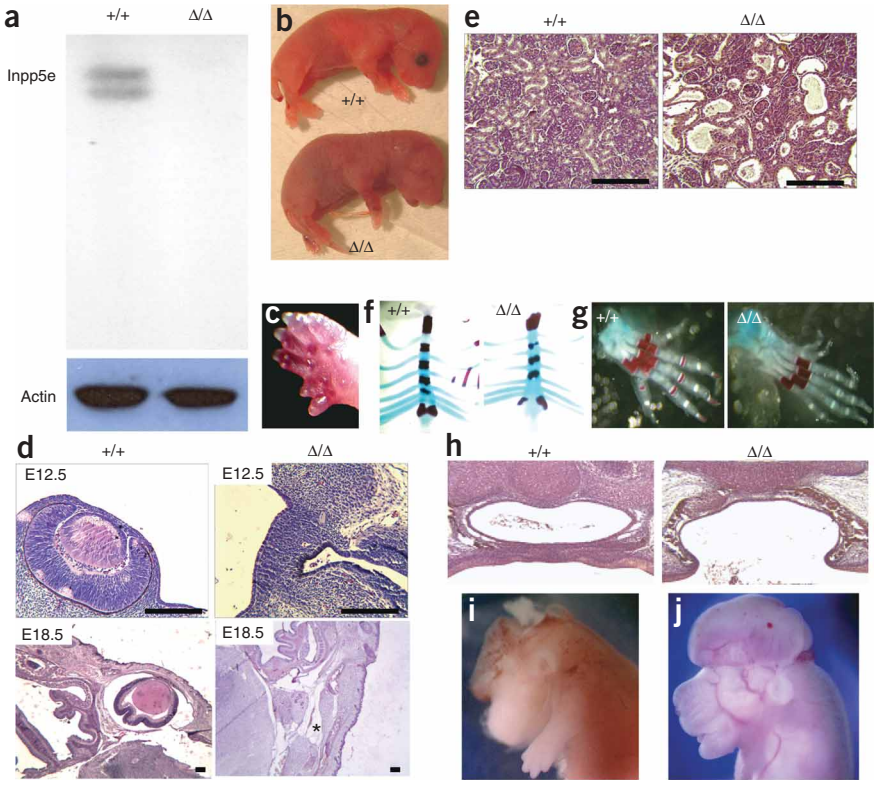

Figure 1 Phenotypic characterization of *Inpp5e*$^{\Delta/\Delta}$ mice. (**a**) Protein blot analysis on E13.5 brain protein extracts with a rabbit polyclonal antibody directed against the N-terminal end of the mouse Inpp5e protein. No Inpp5e is detected in brain from *Inpp5e*$^{\Delta/\Delta}$ mice. Actin served as a loading control. Similar conclusions were drawn from protein blot analysis on protein extracts from ciliated *Inpp5e*$^{\Delta/\Delta}$ MEFs (data not shown) and from immunofluorescence analysis of ciliated *Inpp5e*$^{\Delta/\Delta}$ MEFs (**Fig. 2d**). (**b**) General appearance and anophthalmia in E18.5 *Inpp5e*$^{\Delta/\Delta}$ embryos. (**c**) Postaxial hexadactyly in E18.5 *Inpp5e*$^{\Delta/\Delta}$ embryo. (**d**) Eye development in E12.5 and E18.5 *Inpp5e*$^{+/+}$ (left) and *Inpp5e*$^{\Delta/\Delta}$ (right) embryos. Mutant embryos show developmental arrest at the optic vesicle stage before appearance of the optic cup. No eye is detected in E18.5 *Inpp5e*$^{\Delta/\Delta}$ embryos (asterisk indicates the normal location of the eye). (**e**) Multiple cysts on kidney section of E18.5 *Inpp5e*$^{\Delta/\Delta}$ embryos. (**f**,**g**) Bifid sternum and delayed ossification of sternum, metacarpals and phalanges in E18.5 *Inpp5e*$^{\Delta/\Delta}$ embryos. Cartilage is stained in blue (alcian blue) and bone in red (alizarin red). The ossified surface is significantly decreased on *Inpp5e*$^{\Delta/\Delta}$ sternum (**f**) and metacarpals and phalanges (**g**) as compared with *Inpp5e*$^{+/+}$ embryos (64–86% of control embryos, $P < 0.005$). (**h**) Frontal section of head showing cleft palate in E18.5 *Inpp5e*$^{\Delta/\Delta}$ embryos. (**i**,**j**) Example of anencephaly and exencephaly in E13.5-E15.5 *Inpp5e*$^{\Delta/\Delta}$ embryos. Scale bars, 10 μm.

frequently occurred at the cilia tip but was also seen at the base of the cilium or along the ciliary shaft (**Fig. 2b**, right, and **Supplementary Fig. 4a**). Transmission electron microscopy (TEM) confirmed the presence of bulges at the distal ends of the cilia and along the ciliary shafts (**Fig. 2c**). As previously reported in mice and in humans with kidney cysts due to primary cilium defects[12,13], we identified apoptotic cells in the cysts (**Supplementary Fig. 5**). These ciliary defects were not specific for cystic tubules, as abnormal cilia and apoptotic cells were also observed in Bowman's capsule from *Inpp5e*$^{\Delta/\Delta}$ cystic glomeruli (**Supplementary Fig. 4b**,**c**).

We next analyzed the subcellular localization of Inpp5e in mouse embryonic fibroblasts (MEFs). Inpp5e was detected by protein blotting on protein extracts from non-ciliated control MEFs, but no clear subcellular localization was observed by immunofluorescence (**Supplementary Fig. 6a–d**). By contrast, in *Inpp5e*$^{+/+}$ MEFs cultured at confluence for 72 h in the absence of serum to induce the assembly of a primary cilium[14], Inpp5e was concentrated in the cilium and co-localized with acetylated α-tubulin and PDGFRα, two markers of the ciliary axoneme in ciliated MEFs[14] (**Fig. 2d** and **Supplementary Fig. 6c**,**d**). Under the same conditions, a primary cilium with a normal morphology but lacking the 5-phosphatase protein was also present in *Inpp5e*$^{\Delta/\Delta}$ MEFs (**Fig. 2d**). Quantitative analyses of serum-starved control and mutant MEFs revealed that a similar percentage (~70%) of cells assembled a cilium, suggesting that Inpp5e is not needed for the production of a primary cilium in MEFs (**Fig. 3a**).

Next, we investigated whether stimulating growth factor signaling in MEFs with pre-established cilia might reveal a role for ciliary Inpp5e in the maintenance of this organelle (**Fig. 3a**). Treatment of serum-starved ciliated MEFs with 10% serum for 4 h had no effect on the percentage of pre-established cilia in *Inpp5e*$^{+/+}$ MEFs but caused a significant percentage of *Inpp5e*$^{\Delta/\Delta}$ MEFs to lose their cilia. The serum effect was prevented by the PI3K inhibitor LY294002 (**Fig. 3a**). SEM of *Inpp5e*$^{\Delta/\Delta}$ MEFs 4 h after serum addition revealed that the remaining cilia were short with a dilated appearance, as in kidney cysts (**Supplementary Fig. 7**). These results indicate that the MEF model mimics the structural primary cilium defects observed in *Inpp5e*$^{\Delta/\Delta}$ kidney, and that loss of ciliary Inpp5e sensitizes quiescent MEFs to resorb pre-established cilia in response to one or more factors in serum that signal via the PI3K pathway. Factors known to activate the PI3K pathway, such as IGF-1 (10 nM), insulin (200 nM), EGF (50 ng/ml), FGF (100 ng/ml), PDGF-AA (50 ng/ml) and PDGF-BB (50 ng/ml), individually had no significant effect on the stability of the cilium ($P > 0.15$). However, when testing different growth factor combinations, we found that PDGF-AA, which signals through its alpha receptor (PDGFRα) localized on the cilium membrane in ciliated MEFs (**Fig. 2d** and ref. 14), was necessary to induce ciliary instability (**Fig. 3a**). Stimulation of *Inpp5e*$^{\Delta/\Delta}$ MEFs by PDGF-AA and either IGF-1, EGF or FGF rapidly destabilized the cilium, whereas stimulation by IGF-1 + EGF + FGF did not (**Fig. 3a**). Blocking ciliary PDGFRα signaling with a neutralizing antibody significantly prevented ciliary instability in serum- or PDGF-AA + EGF-stimulated *Inpp5e*$^{\Delta/\Delta}$ MEFs (**Fig. 3a**). This indicates that ciliary instability in *Inpp5e*$^{\Delta/\Delta}$ MEFs requires the combined activation of ciliary PDGFRα and other growth factor receptors expressed on the outside of the cilium, such as EGF or IGF-1 receptors[14]. These results also indicate that signaling downstream of ciliary PDGFRα is tightly controlled at the PtdIns(3,4,5)P3 level by ciliary phosphoinositide 5-phosphatase Inpp5e. Because this pathway controls cell cycle entry in ciliated MEFs[14], we analyzed the percentage of cells in different phases of the cell cycle 24 h after serum stimulation (**Fig. 3b**). As a consequence of Inpp5e inactivation, a significantly higher percentage

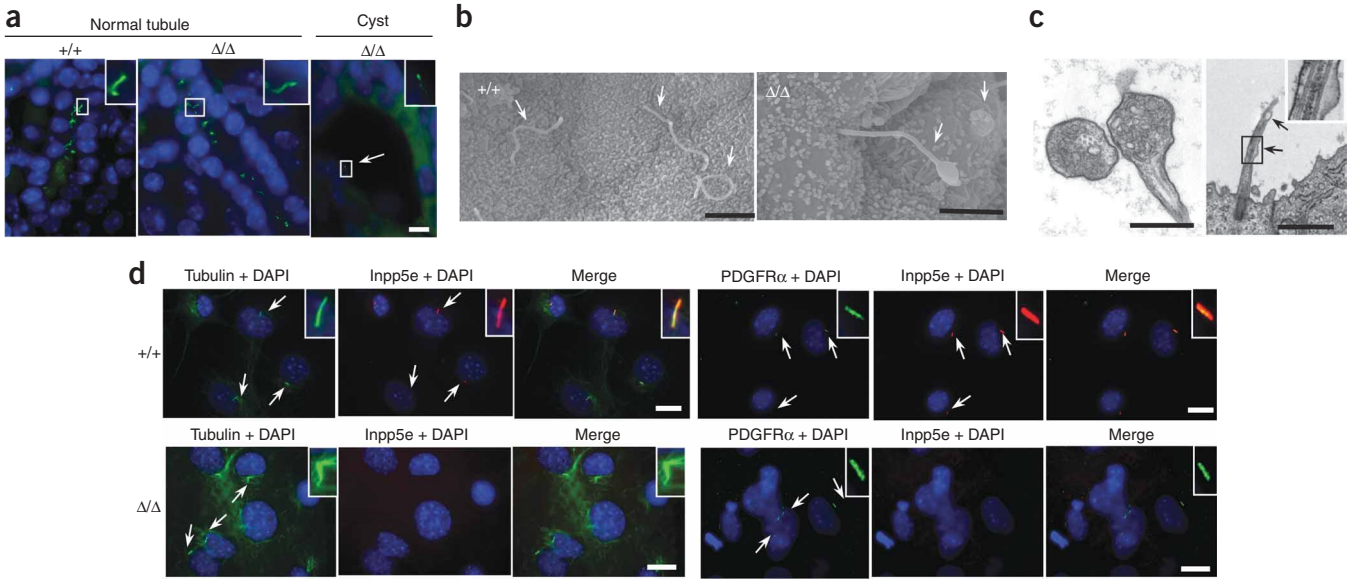

Figure 2 Primary cilium alterations and Inpp5e localization. (**a**) Immunofluorescence studies with an antibody to acetylated α-tubulin, a marker of the primary cilium (green), on kidney tubule cells from a E18.5 *Inpp5e*$^{+/+}$ embryo (left) and on cells lining a normal tubule (center) or a cyst (right) from a E18.5 *Inpp5e*$^{\Delta/\Delta}$ embryo. A unique cilium is visible in the cyst (arrow). Number and length of primary cilia were analyzed in ten tubules or cysts per kidney section, four sections per mouse, two mice per genotype. Insets, high magnification of a primary cilium. Nuclei are stained with DAPI (blue). Scale bars, 5 μm. (**b**) SEM views of primary cilia (arrows) protruding from *Inpp5e*$^{+/+}$ renal tubular cells (left) and from *Inpp5e*$^{\Delta/\Delta}$ cells lining a kidney cyst (right). Scale bars, 2 μm. (**c**) TEM views of a bulge at the tip of a primary cilium (left) and along the ciliary shaft (arrows and inset) in *Inpp5e*$^{\Delta/\Delta}$ cells lining a kidney cyst. The bulges usually contained vesicular structures with electron-dense material. Scale bars, 0.5 μm. (**d**) Immunofluorescence studies on *Inpp5e*$^{+/+}$ (above) and *Inpp5e*$^{\Delta/\Delta}$ (below) MEFs with antibodies directed against two primary cilium markers (acetylated α-tubulin or PDGFRα, green) and a rabbit polyclonal antibody directed against the N terminus of mouse Inpp5e (red). Inpp5e is exclusively expressed in the ciliary axoneme of control MEFs. No Inpp5e protein is detected in *Inpp5e*$^{\Delta/\Delta}$ MEFs. Arrows indicate cilia. Nuclei are stained with DAPI (blue). Insets show higher-magnification images. Scale bars, 5 μm.

of *Inpp5e*$^{\Delta/\Delta}$ MEFs were in the S and the G2/M phases of the cell cycle as compared with *Inpp5e*$^{+/+}$ MEFs.

To analyze the effects of Inpp5e inactivation in adult mice, we crossed *Inpp5e*$^{flox/\Delta}$ mice with *CAGG-Cre-ER*^{TM} transgenic mice expressing a tamoxifen-inducible form of Cre recombinase in several tissues[15]. *Inpp5e*$^{flox/\Delta}$ *CAGG-Cre-ER*^{TM} mice were indistinguishable from control mice. Tamoxifen injection in 4-week-old *Inpp5e*$^{flox/\Delta}$ *CAGG-Cre-ER*^{TM} mice had no effect on survival at 6 months. However, the tamoxifen-treated mice showed significantly greater body weight (control male mice: 30.75 ± 1.34 g; tamoxifen-treated *Inpp5e*$^{flox/\Delta}$ *CAGG-Cre-ER*^{TM} male mice: 38.70 ± 1.66 g; mean ± s.d.), which is a feature of ciliopathies[9–11]. The retinal photoreceptor cell layer of tamoxifen-treated *Inpp5e*$^{flox/\Delta}$ *CAGG-Cre-ER*^{TM} mice was completely absent, indicating that Inpp5e inactivation in adult mice results in a severe retinal dystrophy, another feature of ciliopathies (**Supplementary Fig. 8a**). We also discovered cystic glomeruli on

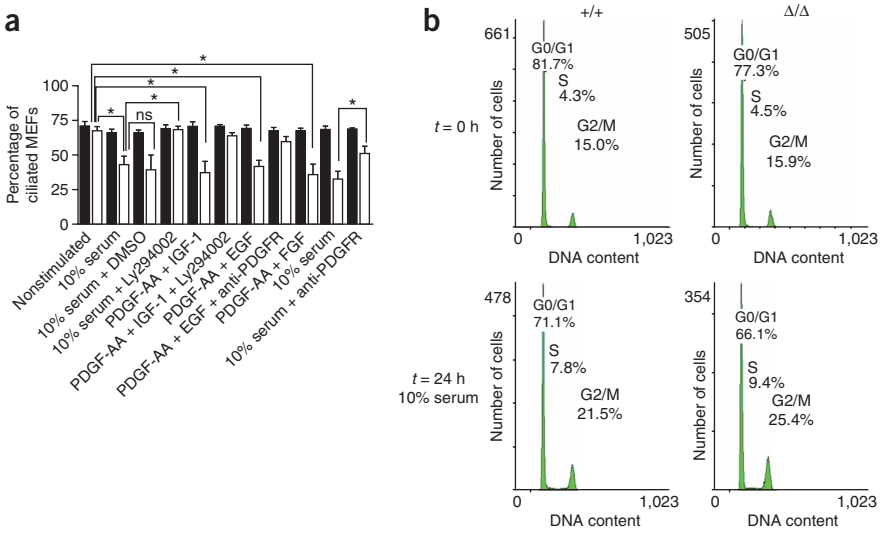

Figure 3 Role of Inpp5e in primary cilium stability. (**a**) Percentages of ciliated *Inpp5e*$^{+/+}$ (black bars) and *Inpp5e*$^{\Delta/\Delta}$ (white bars) MEFs when cultured in the absence of serum or growth factors, and when stimulated with 10% serum or different combinations of growth factors for 4 h, supplemented or not with the PI3K inhibitor Ly294002 or its solvent or with the neutralizing antibody to PDGFRα. At least 100 cells were analyzed per condition and per experiment. Results represent means ± s.d. of four independent experiments. Statistics: $*P <$ 0.005; ns, not significant. (**b**) Cell cycle entry of ciliated MEFs following serum stimulation. *Inpp5e*$^{+/+}$ (left) and *Inpp5e*$^{\Delta/\Delta}$ (right) ciliated MEFs were stimulated for 24 h ($t = 24$ h) or not ($t = 0$ h) with 10% serum, incubated with propidium iodide and analyzed by flow cytometry. The percentage of cells in the G0/G1, S and G2/M phases of the cycle are indicated. Results are representative of three independent experiments. As compared with *Inpp5e*$^{+/+}$ MEFs, the number of cells in the G0/G1 phase was significantly decreased in *Inpp5e*$^{\Delta/\Delta}$ MEFs ($P < 0.04$), and the number of cells in S or G2/M phases was significantly increased in *Inpp5e*$^{\Delta/\Delta}$ MEFs ($P < 0.04$ and $P < 0.01$, respectively).

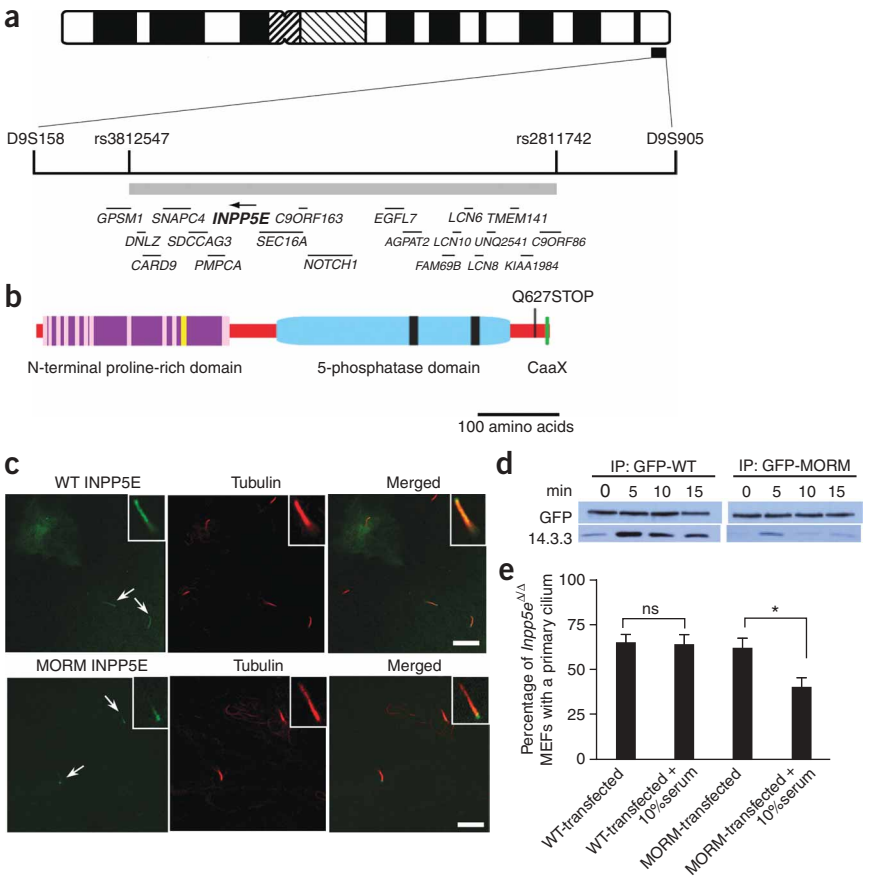

Figure 4 Studies of human INPP5E. (**a**) Linkage to the 9qter region (size: 750 kb and 2.1cM) is shown with defining polymorphic microsatellites D9S158 and D9S905. A homozygous concordant minimum critical region of 480 kb (gray bar flanked by markers rs3812547 and rs2811742) was defined in all affected individuals by typing 17 SNPs and two polymorphic microsatellites across the region. All genes within the MORM critical interval are shown as bars, except *INPP5E* shown as an arrow. (**b**) INPP5E protein, showing known domains and the MORM Q627STOP mutation. The N-terminal proline-rich domain (purple rectangle) is comprised of an SH3-binding class I proline-rich motif (yellow) and 12 PXXP motifs (pink). The 5-phosphatase signature domains (black bars) are shown within the 5-phosphatase domain (blue rectangle). The C-terminal CaaX motif (where C is a cysteine residue, aa are two small, generally aliphatic residues, and X is any amino acid[23], green bar) and the site of the MORM nonsense mutation (vertical line) in the last exon of *INPP5E* are indicated. (**c**) Ciliary localization of GFP-tagged wild-type and MORM INPP5E in hTERT-RPE1 cells. hTERT-RPE1 cells were transfected with GFP-tagged INPP5E expression vectors (arrows indicate cilia, green), starved for three days to induce ciliogenesis and stained with an antibody to acetylated α-tubulin to detect the primary cilium (red). At least 100 GFP-positive hTERT-RPE1 cells were analyzed per experiment for GFP protein localization. Three independent experiments were performed. Similar results were obtained using HA-tagged INPP5E proteins (data not shown). Scale bars, 10 μm. Insets show higher-magnification images. (**d**) Analysis of INPP5E and 14-3-3 protein interaction in hTERT-RPE1 cells. hTERT-RPE1 cells were transfected with GFP-tagged wild-type or MORM INPP5E expression vectors, serum-starved for 24 h to induce ciliogenesis and stimulated or not with 10% serum for 5, 10 and 15 min. After cell lysis, an antibody to GFP was used to immunoprecipitate GFP-INPP5E protein complexes, and a western blot analysis was performed using an antibody to 14-3-3. Immunoprecipitated GFP–wild-type and GFP-MORM proteins served as loading controls. (**e**) Effect of INPP5E expression on the primary cilium stability defect in *Inpp5e*$^{\Delta/\Delta}$ MEFs. An antibody to acetylated α-tubulin was used to detect the primary cilium in GFP-tagged wild-type and MORM INPP5E–transfected *Inpp5e*$^{\Delta/\Delta}$ MEFs treated or not with 10% serum for 4 h. The percentage of GFP-positive *Inpp5e*$^{\Delta/\Delta}$ MEFs with a primary cilium is represented. At least 100 GFP-positive *Inpp5e*$^{\Delta/\Delta}$ MEFs were analyzed per experiment for the presence of a cilium. Similar results were obtained when stimulating *Inpp5e*$^{\Delta/\Delta}$ MEFs with PDGF-AA + EGF (data not shown). Results are means ± s.d. of four independent experiments. Statistics: $^*P < 0.005$; ns, not significant.

kidney sections from 6-month-old tamoxifen-treated *Inpp5e*$^{flox/\Delta}$ *CAGG-Cre-ER*^{TM} mice, as described in other ciliary protein defects[16] (**Supplementary Fig. 8b**).

MORM syndrome is an autosomal recessive disorder characterized by mental retardation, obesity, congenital retinal dystrophy and micropenis in males[17]. This phenotype is similar to but distinct from Bardet-Biedl syndrome[18]. We previously defined linkage of a family with MORM syndrome to a subtelomeric region on chromosome 9q34.3 (ref. 17). Assembly of a contig of the region and analyses of encompassed microsatellites refined the minimum region but failed to reveal an informative homozygous genomic segment (**Fig. 4a**). We sequenced 14 of the genes within the MORM candidate region. Analysis of exonic SNPs revealed a homozygous informative region of 480 kb shared by all affected individuals (**Fig. 4a**). Within this region, we found a single unreported change, c.1879C>T in the terminal exon of *INPP5E*. This change segregated with MORM within the family and was not present in 200 ethnically matched controls. The mutation is predicted to cause premature truncation of the protein with the omission of the terminal 18 amino acids and thus causes loss of the C-terminal CaaX domain, which is conserved in all mammalian and avian INPP5E proteins (**Fig. 4b** and **Supplementary Fig. 9**). The CaaX domain often encodes a motif for addition of a geranylgeranyl or farnesyl lipid group to the cysteine leading to membrane targeting of the protein, such as occurs with the type 1 InsP3 5-phosphatase[19].

To study the consequence of the mutation, we tagged human wild-type and MORM INPP5E proteins at their N-terminal end with green fluorescent protein (GFP) or hemagglutinin A (HA) peptides and expressed them in cells. We first determined the ciliary localization of the INPP5E proteins in the ciliated human retinal pigment epithelial hTERT-RPE1 cell line (**Fig. 4c**). Among the cells transfected with wild-type INPP5E, more than 80% showed even distribution of the INPP5E protein along the cilial axoneme. By contrast, only 16% of MORM INPP5E–transfected cells had such uniform distribution of the protein, whereas 84% showed MORM INPP5E expression that was limited to one extremity of the cilium. These results indicate that the terminal 18 amino acids of INPP5E are important for normal ciliary localization in these cells (**Fig. 4c**). Another consequence of INPP5E truncation was a relative inability to interact with and immunoprecipitate 14-3-3 proteins when overexpressed in ciliated hTERT-RPE1 cells (**Fig. 4d**).

We then tested INPP5E catalytic activity in COS-7 cells with phosphatidylinositol (3,4,5)-trisphosphate (PtdIns(3,4,5)P3) and PtdIns(4,5)P2 as substrates. We observed a similar activity for the wild-type and MORM INPP5E proteins, demonstrating that the truncated protein retains its 5-phosphatase activity (**Supplementary Fig. 10**). Finally, we analyzed the capacity of these human proteins to rescue the primary cilium stability defect of *Inpp5e*$^{\Delta/\Delta}$ MEFs (**Fig. 4e**) by transfecting the MEFs in serum-free medium to induce ciliogenesis and 3 d later treating them with 10% serum for 4 h. The percentage of ciliated cells among *Inpp5e*$^{\Delta/\Delta}$ MEFs transfected with wild-type INPP5E was similar before and after serum stimulation (**Fig. 4e**), whereas the percentage of ciliated cells in those transfected with MORM INPP5E decreased significantly after serum stimulation (**Fig. 4e**). Together, these experiments show that MORM INPP5E has diminished capacity to stabilize the primary cilium, which is likely due to its defect in ciliary localization and protein interaction. Despite its intact enzymatic activity, MORM INPP5E expression in the outside of the cilium is not sufficient to perform this stabilization function.

Depending on the presence and concentration of growth factors or other mitotic signals, primary cilia are assembled and stabilized in quiescent/differentiated cells and disassembled before entry into the next cell division. Our results show that ciliary Inpp5e functions to stabilize the normal structure and number of primary cilia in quiescent cells stimulated by growth factors. They also indicate that activation of the ciliary PI3K signaling pathway by growth factors such as PDGF-AA must be tightly controlled in the ciliary axoneme to prevent premature entry into the cell cycle and disassembly of the primary cilium. The presence of the PtdIns(3,4,5)P3 5-phosphatase Inpp5e in the ciliary axoneme is essential to this control. Inactivation or ciliary mislocalization of Inpp5e may lead primarily to increased PDGF-AA–PDGFRα–PI3K ciliary signaling and, together with extra-ciliary growth factor signals, to cell cycle entry. Secondarily, the increased ciliary sensitivity to growth factor stimulation and premature cell cycle entry most likely affect ciliary stability, resulting in ciliopathies. Cell cycle arrest associated with decreased PtdIns(3,4,5)P3 levels and Akt phosphorylation were reported in Inpp5e-overexpressing cells stimulated by serum or PDGF[20], which supports this hypothesis. Another possibility is that the decreased stability of the primary cilium in Inpp5e-deficient cells could result from the more direct mechanism of altered levels of ciliary PtdIns(4,5)P2 levels, the second substrate for Inpp5e. Molecularly, the consequences of altered ciliary PtdIns(4,5)P2 levels are difficult to predict, but they may include abnormal localization and/or function of essential ciliary proteins known to bind phospholipids, such as tubby and BBS5 proteins[21,22]. Together, the Inpp5e-related ciliopathies we describe here reveal the importance of the tight control of ciliary phosphoinositide metabolism in mammalian development and maintenance of tissue integrity in adulthood.

METHODS

Methods and any associated references are available in the online version of the paper at http://www.nature.com/naturegenetics/.

Note: Supplementary information is available on the Nature Genetics website.

ACKNOWLEDGMENTS

We thank C. Erneux, C. Moreau, F. Fontaine and L. Cuvelier for discussions and technical help, S.J. Elledge for the recombineering reagents, A. de Kerchove d'Exaerde for help with the design of the oligonucleotide probes, A. Nagy for the R1 ES cells, A.P. McMahon for the *CAGG-Cre-ER*^{TM} mice and E. Golemis for hTERT-RPE1 cells. This work was supported by the Fonds de la Recherche Scientifique-FNRS (FRS-FNRS; to S.G. and S.S.), the Fonds pour la Formation à la Recherche dans l'Industrie et dans l'Agriculture (FRIA; to M.J., M.B. and E.P.), the Fonds de la Recherche Scientifique Médicale (FRSM; to S.S. and S.N.S.), the Fondation Rose et Jean Hoguet (to E.P.), Action de Recherches Concertée de la Communauté Française de Belgique (to S.N.S., S.S. and M.B.), The Queen Elisabeth Medical Fundation (to S.N.S.), the Fonds David et Alice Van Buuren (to M.J.), the Royal Society and Cancer Research UK (to F.G.), the American Heart Association (0730350N; to M.V.K.), the US National Institutes of Health (HL16634; to M.V.K.) and the Wellcome Trust (to J.J.C. and C.G.W).

AUTHOR CONTRIBUTIONS

All authors designed the experiments; M.J., J.J.C., S.G., D.J.H., M.B., E.P., P.C. and D.P.-M. performed experiments; all authors analyzed data; M.J., M.A., M.V.K., F.G., J.H.R. and C.G.W. provided essential reagents and/or biological samples; all authors discussed the results; and S.S. wrote the manuscript with J.J.C. and C.G.W.'s help with the first draft.

Published online at http://www.nature.com/naturegenetics/.
Reprints and permissions information is available online at http://npg.nature.com/reprintsandpermissions/.

1. Adams, M., Smith, U.M., Logan, C.V. & Johnson, C.A. Recent advances in the molecular pathology, cell biology and genetics of ciliopathies. *J. Med. Genet.* **45**, 257–267 (2008).
2. Christensen, S.T., Pedersen, L.B., Schneider, L. & Satir, P. Sensory cilia and integration of signal transduction in human health and disease. *Traffic* **8**, 97–109 (2007).
3. Anderson, C.T. *et al.* Primary cilia: cellular sensors for the skeleton. *Anat. Rec.* **291**, 1074–1078 (2008).
4. Blero, D., Payrastre, B., Schurmans, S. & Erneux, C.E. Phosphoinositide phosphatases in a network of signaling reactions. *Pflugers Arch.* **455**, 31–44 (2007).
5. Astle, M.V., Horan, K.A., Ooms, L.M. & Mitchell, C.A. The inositol polyphosphate 5-phosphatases: traffic controllers, waistline watchers and tumour suppressors? *Biochem. Soc. Symp.* **74**, 161–181 (2007).
6. Asano, T., Mochizuki, Y., Matsumoto, K., Takenawa, T. & Endo, T. Pharbin, a novel inositol polyphosphate 5-phosphatase, induces dendritic appearances in fibroblasts. *Biochem. Biophys. Res. Commun.* **261**, 188–195 (1999).
7. Kisseleva, M.V., Wilson, M.P. & Majerus, P.W. The isolation and characterization of a cDNA encoding phospholipids specific inositol polyphosphate 5-phosphatase. *J. Biol. Chem.* **275**, 20110–20116 (2000).
8. Kong, A.M. *et al.* Cloning and characterization of a 72-kDa inositol-polyphosphate 5-phosphatase localized to the Golgi network. *J. Biol. Chem.* **275**, 24052–24064 (2000).
9. Pan, J., Wang, Q. & Snell, W.J. Cilium-generated signalling and cilia-related disorders. *Lab. Invest.* **85**, 452–463 (2005).
10. Singla, V. & Reiter, J.F. The primary cilium as the cell's antenna: signalling at a sensory organelle. *Science* **313**, 629–633 (2006).
11. Badano, J.L., Mitsuma, N., Beales, P.L. & Katsanis, N. The ciliopathies: an emerging class of human genetic disorders. *Annu. Rev. Genomics Hum. Genet.* **7**, 125–148 (2006).
12. Ong, A.C. & Wheatley, D.N. Polycystic kidney disease: the ciliary connection. *Lancet* **361**, 774–776 (2003).
13. Lin, F. *et al.* Kidney-specific inactivation of the KIF3A subunit of kinesin-II inhibits renal ciliogenesis and produces polycystic kidney disease. *Proc. Natl. Acad. Sci. USA* **100**, 5286–5291 (2003).
14. Schneider, L. *et al.* PDGFRαα signaling is regulated through the primary cilium in fibroblasts. *Curr. Biol.* **15**, 1861–1866 (2005).
15. Hayashi, S. & McMahon, A.P. Efficient recombination in diverse tissues by a tamoxifen-inducible form of Cre: a tool for temporally regulated gene activation/inactivation in the mouse. *Dev. Biol.* **244**, 305–318 (2002).
16. Phillips, C.L. *et al.* Renal cysts in *inv/inv* mice resemble infantile nephronophthisis. *J. Am. Soc. Nephrol.* **15**, 1744–1755 (2004).
17. Hampshire, D.J. *et al.* MORM syndrome (mental retardation, truncal obesity, retinal dystrophy and micropenis), a new autosomal recessive disorder, links to 9q34. *Eur. J. Hum. Genet.* **14**, 543–548 (2006).
18. Beales, P.L., Warner, A.M., Hitman, G.A., Thakker, R. & Flinter, F.A. Bardet-Biedl syndrome: a molecular and phenotypic study of 18 families. *J. Med. Genet.* **34**, 92–98 (1997).
19. De Smedt, F., Boom, A., Pesesse, X., Schiffmann, S.N. & Erneux, C.E. Post-translational modification of human brain type I inositol-1,4,5-trisphosphate 5-phosphatase by farnesylation. *J. Biol. Chem.* **271**, 10419–10424 (1996).
20. Kisseleva, M.V., Cao, L. & Majerus, P.W. Phosphoinositide-specific inositol polyphosphate 5-phosphatase IV inhibits Akp/protein kinase B phosphorylation and leads to apoptotic cell death. *J. Biol. Chem.* **277**, 6266–6272 (2002).
21. Santagata, S. *et al.* G-protein signalling through tubby proteins. *Science* **292**, 2041–2050 (2001).
22. Nachury, M.V. *et al.* A core complex of BBS proteins cooperates with the GTPase Rab8 to promote ciliary membrane biogenesis. *Cell* **129**, 1201–1213 (2007).
23. Lane, K.T. & Beese, L.S. Structural biology of protein farnesyltransferase and geranylgeranyltransferase type I. *J. Lipid Res.* **47**, 681–699 (2006).

ONLINE METHODS

Production of *Inpp5e*$^{flox/+}$ and *Inpp5e*$^{\Delta/+}$ mice. A targeting vector containing a first *loxP* site inserted in intron 6 of the murine *Inpp5e* gene as well as a second *loxP* site and a neomycin-resistance cassette (*neo*^{R}) flanked by *FRT* sites inserted in intron 8 of the same gene was constructed following a previously described method[24]. Briefly, screening of a λKO-2 129/SvEvBrd mouse genomic DNA library in a λ phagemid with a 510-bp radiolabeled genomic DNA fragment encompassing exon 6 of the murine *Inpp5e* gene as a probe yielded two positive λ clones with a ~12-kb genomic DNA fragment containing both introns 6 and 8 of the *Inpp5e* gene. In a first round of recombination, one of the λ clones was used to infect SCRN10 bacteria containing the pML179-*loxP*-*tet*^{R}-*loxP* plasmid in order to insert the *loxP*-*tet*^{R}-*loxP* DNA fragment in intron 6 of the gene. Infection of JM107-RS bacteria with the resulting recombinant λ phagemid yielded the corresponding recombinant plasmid. In a second round of recombination, 294-Cre bacteria, which constitutively express the Cre recombinase, were electroporated with the above recombinant plasmid to eliminate the *tet*^{R} cassette and one of the *loxP* sites from the plasmid, leaving a unique *loxP* site in intron 6 of the construct. Then, in a third round of recombination, the *loxP*-*FRT*-*neo*^{R}-*kana*^{R}-*FRT* DNA fragment was inserted in intron 8 of the *Inpp5e* gene fragment present in the plasmid by electroporation of pML104/DH10B bacteria (**Supplementary Fig. 1**). The linearized plasmid was electroporated into R1 ES cells, and *neo*^{R} ES cell clones were isolated after 6 d of culture. ES cell clone DNA was analyzed by PCR and DNA blotting to detect homologous recombinant events (**Supplementary Fig. 1**). Chimeric mice were obtained after aggregation of positive ES cell clones with CD-1 morulae. Chimeric mice that transmitted the modified *Inpp5e* allele to their progeny were crossed with PGK-Cre- or PGK-Flp-recombinase–transgenic mice to generate *Inpp5e*$^{\Delta/+}$ and *Inpp5e*$^{flox/+}$ mice, respectively. For conditional inactivation of *Inpp5e* in adult mice, *Inpp5e*$^{flox/+}$ mice were crossed with *CAGG-Cre-ER*^{TM} tamoxifen-inducible Cre mice, where the Cre recombinase is downstream of the chicken *Actb* (β-actin) promoter and cytomegalovirus immediate-early enhancer[25]. Mice 4-weeks-old were intraperitoneally injected with 9 mg tamoxifen per 40 g body weight per day for 5 consecutive days. Sequences of the PCR primers to detect the wild-type, *loxP*-flanked and $^{\Delta}$*Inpp5e* alleles are available on request. All mouse studies were authorized by the Animal Care Use and Review Committee of the Université Libre de Bruxelles.

Reagents. LY294002, PDGF-AA and PDGF-BB were from Sigma, EGF, IGF-1 and FGF were from Upstate and insulin was from Novo Nordisk.

Antibodies, protein blotting, immunofluorescence and immunohistochemistry. An antibody to mouse Inpp5e (anti–mouse Inpp5e) was raised in rabbit after immunization with the N-terminal MLQGQPPNTEKKLIP peptide (Eurogentec) and affinity-purified. Specificity of the antibody was confirmed by preincubation with an excess amount of the immunization peptide in immunofluorescence studies on *Inpp5e*$^{+/+}$ ciliated MEFs (**Supplementary Fig. 11a**) as well as in protein blot analysis on brain protein extracts from *Inpp5e*$^{+/+}$ mice (**Supplementary Fig. 11b**) and on COS-7 cell extracts expressing the recombinant Inpp5e protein (**Supplementary Fig. 11c**). The anti–acetylated α-tubulin (clone 6-11B-1), the anti–γ-tubulin, the anti-AQP2 (A7310) and the anti–HA were from Sigma. The anti-GFP rabbit polyclonal, serum and IgG Fab (A11122), biotin-conjugated anti–rabbit IgG, FITC- or biotin-conjugated anti–mouse-IgG, Alexa-594–streptavidin, Alexa-488–anti-rabbit and Alexa-555–anti-mouse antibodies were all from Invitrogen. The goat anti–mouse PDGFRα neutralizing antibody (clone AF1062) was from R&D Systems; the anti–14-3-3β (H8) monoclonal antibody, which recognizes all isoforms of the 14-3-3 family (sc-1657), from Santa Cruz Biotechnology; and the anti-AQP1 (ab65837) from Abcam. Nuclei were labeled with DAPI or propidium iodide.

Cell cycle entry analysis. *Inpp5e*$^{+/+}$ and *Inpp5e*$^{\Delta/\Delta}$ ciliated MEFs were stimulated with 10% serum for 24 h, harvested, fixed overnight in ethanol, incubated with propidium iodide and analyzed by flow cytometry on a FC 500 cytometer (Beckman Coulter) to determine cellular DNA content.

TUNEL assay. An *in situ* cell death detection kit from Roche was used to detect apoptotic cells on kidney sections.

Malachite phosphatase assay. COS-7 cells were transfected with GFP-tagged wild-type or MORM INPP5E expression plasmids and lysed. GFP-tagged proteins were immunoprecipitated using a rabbit anti-GFP, washed and engaged in the malachite green dye phosphatase assay[26]. Protein blot analysis of the immunoprecipitates confirmed that the same amount of wild-type or MORM INPP5E proteins was engaged in the reaction. Then, PtdIns(3,4,5)P3-di-C8 or PtdIns(4,5)P2di-C8 (Cell Signals Inc.) was added to the immunoprecipitates in the assay buffer at 37 °C. After 10 min, reactions were stopped with EDTA and boiled at 100 °C. Next, malachite green reagent was added for an additional 10 min. Absorbance was measured at 650 nm. Inorganic phosphate release was quantified by comparison to a standard curve of KH_2PO_4 in water. The data are means of triplicates ± s.d.

Human molecular genetic studies. Ethical approval for this project was obtained in both UK and Pakistan; informed consent was obtained from participants as described in reference 17. DNA was extracted from blood samples from family members by standard methods. SNPs and polymorphic markers were chosen from the MORM linkage region from the Human Genome Browser and analyzed as described[17]. Genes within the MORM region were identified from the Human Genome Browser. Primers were designed to amplify all exons and splice sites by use of the Human Genome Browser, Entrez Gene, Primer3 and BLAST. Genomic DNA from family members was bidirectionally sequenced and the results assessed by Chromas, BLAST and against reference sequences. The MORM mutation was excluded from ethnically matched controls by bidirectional sequencing of genomic DNA. Protein domains and motifs were sought using SMART, Prosite and Pfam. Evolutionary comparison of INPP5E proteins was by BLAST and UCSC Genome Browsers.

Expression vectors and transfections. A human *INPP5E* cDNA clone (BC028032) was used as a template in PCR reactions to generate the *INPP5E* expression constructs. Sequences of the primers for GFP-WT *INPP5E*, GFP-MORM *INPP5E*, HA-WT *INPP5E* and HA-MORM *INPP5E* are presented in **Supplementary Table 1**. The PCR fragments were digested and ligated into pcDNA3 (Invitrogen). Expression constructs were sequenced to verify success of the cloning. In overexpression experiments, hTERT-RPE1 cells or *Inpp5e*$^{\Delta/\Delta}$ MEFs were plated on coverslips in six-well plates. When cells reached ~80% confluency, 1 μg of plasmid DNA was transfected into the cells using Lipofectamine 2000 (Invitrogen) and Plus Reagent (Invitrogen). Three days after transfection, hTERT-RPE1 cells were fixed with 4% paraformaldehyde and stained using the anti–acetylated α-tubulin and, when necessary, the anti-HA described above. Transfected *Inpp5e*$^{\Delta/\Delta}$ MEFs were treated (or not treated) with 10% serum or PDGF-AA + EGF growth factors for 4 h and then processed for primary cilium detection as described above. Slides were analyzed using an LSM510 META confocal microscope and ciliary localization proven by colocalization between INPP5E and the primary cilium marker anti–acetylated α-tubulin. For counting experiments, every transfected cell was scored as to whether a primary cilium was present or absent, and counting ceased for each experiment when at least 100 transfected GFP- or HA-positive cells had been analyzed.

Histology and *in situ* hybridization. Tissues were fixed in 3% paraformaldehyde and embedded in paraffin following standard procedures. Serially cut 5-μm-thick sections were stained with hematoxylin and eosin. The skeleton was fixed in ethanol and stained with alcian blue and alizarin red. For *in situ* hybridization, embryo sections were fixed in paraformaldehyde 4% and incubated with radiolabeled sense or antisense oligonucleotide probes encoded in exon 8 of the murine *Inpp5e* gene (oligonucleotide sequences are presented in **Supplementary Table 1**).

Scanning and transmission electron microscopy morphology studies. For TEM, samples were fixed overnight at 4 °C in 2.5% glutaraldehyde, 0.1 M cacodylate buffer (pH 7.2), and postfixed in OsO_4 (2%) in the same buffer. After serial dehydration in increasing ethanol concentrations, samples were embedded in Agar 100 (Agar Scientific Ltd.) and left to polymerize for three days at 60 °C. Ultrathin sections (50–70 nm thick) were collected on Formvar-carbon–coated copper grids and stained with uranyl acetate and lead citrate. Observations were made on a Tecnai 10 electron microscope (FEI) and images were captured with a MegaView II camera and processed with AnalySIS and Adobe Photoshop

software. For SEM, samples were fixed overnight at 4 °C in 2.5% glutaraldehyde, 0.1 M cacodylate buffer (pH 7.2) and postfixed in OsO_4 (2%) in the same buffer. After serial dehydration in increasing ethanol concentrations, samples were dried at critical point and coated with platinum by standard procedures. Observations were made in a FEI FEG ESEM XL30 (FEI).

Statistical analyses. Student *t*-test and χ^2 test were performed with GraphPad Prism 4.0. For each test, a difference of $P < 0.05$ was considered significant.

24. Zhang, P., Li, M.Z. & Elledge, S.J. Towards genetic genome projects: genomic library screening and gene-targeting vector construction in a single step. *Nat. Genet.* **30**, 31–39 (2002).
25. Hayashi, S. & McMahon, A.P. Efficient recombination in diverse tissues by a tamoxifen-inducible form of Cre: a tool for temporally regulated gene activation/inactivation in the mouse. *Dev. Biol.* **244**, 305–318 (2002).
26. Vandeput, F., Backers, K., Villeret, V., Pesesse, X. & Erneux, C. The influence of anionic lipids on SHIP2 phosphatidylinositol 3,4,5-trisphosphate 5-phosphatase activity. *Cell. Signal.* **18**, 2193–2199 (2006).